COMMUNICATIONS CHEMISTRY

ARTICLE

DOI: 10.1038/s42004-017-0002-y OPEN

In situ generation of intercalated membranes for efficient gas separation

Zixi Kang[1], Sasa Wang[1], Lili Fan[1], Minghui Zhang[1], Wenpei Kang[1], Jia Pang[1], Xinxin Du[1], Hailing Guo[2], Rongming Wang[1] & Daofeng Sun[1]

Membranes with well-defined pore structure which have thin active layers may be promising materials for efficient gas separation. Graphene oxide (GO) materials have potential applications in the field of membrane separation. Here we describe a strategy for the construction of ultra-thin and flexible HKUST-1@GO intercalated membranes, where HKUST-1 is a copper-based metal–organic framework with coordinatively unsaturated metal sites, with simultaneous and synergistic modulation of permeance and selectivity to achieve high H_2/CO_2 separation. CuO nanosheets@GO membranes are fabricated layer-by-layer via repeated filtration cycles, then transformed to HKUST-1@GO membranes upon in situ reaction with linkers. The HKUST-1@GO membranes show enhanced performance for gas separation of H_2/CO_2 mixture. The number of filtration cycles is optimized to obtain H_2 permeance of 5.77×10^{-7} mol m^{-2} s^{-1} Pa^{-1} and H_2/CO_2 selectivity of 73.2. Our work provides a facile strategy for the construction of membranes based on metal–organic frameworks and GO, which may be applied in the preparation of flexible membranes for gas separation applications.

[1] College of Science, China University of Petroleum (East China), Qingdao, 266580 Shandong, People's Republic of China. [2] State Key Laboratory of Heavy Oil Processing, Key Laboratory of Catalysis, China National Petroleum Corp. (CNPC), China University of Petroleum (East China), Qingdao, 266555 Shandong, People's Republic of China. Correspondence and requests for materials should be addressed to D.S. (email: dfsun@upc.edu.cn)

The separation of a gas mixture is a critical process in industrial production. However, it is challenging due to similar molecule sizes and physical properties of the composition[1]. Compared with conventional separation technologies such as adsorption, distillation, and condensation, membrane separation is easily operated, efficient, and environmentally friendly, which has developed rapidly in recent years[2,3]. Material research is a core element to enable stable and scalable membranes for efficient separation[4]. Polymer membranes have been widely used in practical applications because of the easy processing and low cost. However, it has been confirmed that polymer membranes suffer the selectivity/permeability trade-off, and cannot exceed Robeson's upper bound[5–7]. Inorganic microporous membranes, such as zeolite and metal–organic frameworks (MOFs) membranes, simultaneously possess ideal selectivity and permeability because of the uniform pore size[8–11]. Yet the issue of up-scaling and process difficulty has hindered their adaptation into industrial applications[12,13]. Mixed matrix membranes (MMMs) consisting of polymers and microporous fillers are considered as a short-term solution for the deficiencies of innocent polymer and inorganic membranes[14–17].

Recently, several studies have reported membranes created from two-dimensional (2D) materials including graphene oxide (GO), zeolite nanosheets (NS), and MOF NS etc.[18–24]. The exfoliated 2D NS were used as blocks to sustain ultra-thin membrane with remarkably high permeance. Thanks to the low cost and flexibility, GO membrane is a potential candidate of the scalable material for gas separation. Gas molecules permeate the GO membrane through the GO defects and layer gaps[22]. According to the studies of Geim and co-workers, the typical empty interlayer spacing of GO laminar membrane would be expanded when the membrane was immersed in an aqueous solution or with vapor, due to the hydration of oxygen-containing groups on the GO NS[25]. To solve this problem, various nanomaterials and molecules have been intercalated into GO NS to form hybrid structures with tuned layer gaps[26]. However, these doping spices such as organic molecules, polymer chains can only adjust the interspace of GO layers, not sieve mixtures or affect the in-plane defects of GO layers[27,28]. Significant effort should be applied to develop uniform, high-density, subnanosized pores in GO-based membrane for stable performance under realistic operating conditions[29].

In this work, we describe a facile strategy for the construction of MMMs to achieve simultaneous and synergistic modulation of permeance and selectivity. Our strategy is illustrated by the preparation of ultra-thin GO-MOFs-based MMMs, in which GO plays a role of flexible matrix, and is sealed in the intergaps between the MOF crystals, to overcome the solvothermal synthesis and interfacial defects of polycrystalline membrane, while MOFs act as fillers with uniform microporosity to improve the gas separation performance compared with the pristine GO membrane. To achieve this target, MOF materials with nanosized thickness should be prepared and doped into the GO layers, while the 2D morphology of the membrane should also be maintained. In the previous reports, a top–down process has been adopted to fabricate MOF NS, which required a post-purification step[21,24]. On the other hand, bottom–up synthesis of MOF NS is challenging due to the complicated crystal growth process of MOFs[30–32]. Based on the knowledge that MOFs are built by metal centers and organic ligands, several polycrystalline MOF membranes have been constructed on the metal substrate by transforming metal substrates into MOFs such as "twin copper source"[33] and "single nickel source"[34] method. The "metal source" method discussed above can be adopted to nanoscale MOF synthesis by transformation from metal oxide NS[35–38]. For nanomaterials, a wide variety of studies were focused on the morphology control of metal oxide, providing many methods to prepare metal oxide NS[39–44].

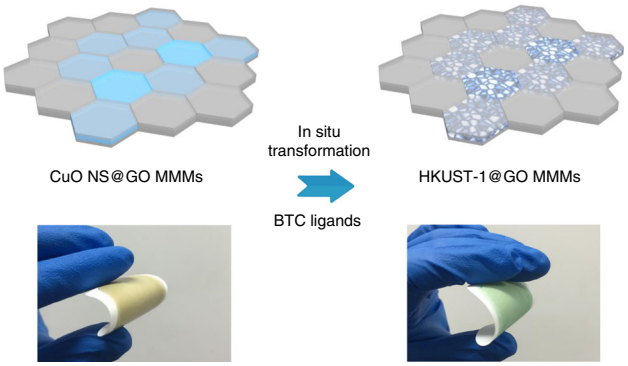

Fig. 1 Schematic illustration of membrane preparation. CuO NS are introduced into the GO membrane to form GuO NS@GO MMMs. A copper MOF (HKUST-1) is grown in situ via reacting with solution-phase ligands. The product is a flexible MMM for gas separation

In this MMM, GO serves as the matrix material to form the main part of the membrane, while HKUST-1 with strong CO_2 affinity acts as a microporous filler. Owing to the 2D morphology of these building blocks, the obtained HKUST-1@GO MMMs possess considerable flexibility as shown in Fig. 1. This flexibility may help to create membranes on the support of hollow fibers, which are efficient modules for gas separation[16]. Permeance tests for single and mixture gases are carried out on the HKUST-1@GO MMMs, demonstrating high permeance and selectivity. As all the MOFs contain metal centers, this strategy may be widely extended to other MOF structures with varied functional groups and pore sizes, providing suitable MMMs for different separation applications.

Results

Preparation of the HKUST-1@GO membranes. CuO NS were first fused into GO via a layer-by-layer method, creating an MMM based on CuO NS and GO, referred as CuO NS@GO (Fig. 1). In the next step, HKUST-1@GO membranes were obtained through an in situ transformation of CuO NS@GO in 1,3,5-benzenetricarboxylic acid (BTC) ligand solution. CuO NS was synthesized by a facial precipitation process[39]. The morphology and structure characterization for CuO NS are presented in Fig. 2 and Supplementary Figure 1. We can learn from the atomic force microscopy (AFM) and transmission electron microscope (TEM) images that the piece diameter was in the range of 0.2–5 μm, while the thickness is around 4 nm (Fig. 2c). More AFM, scanning electron microscope (SEM), and TEM images of CuO NS can be found in Supplementary Figure 1. The TEM and electron diffraction patterns in Fig. 2d indicated the pure phase of CuO NS, which was also proved by the powdered X-ray diffraction (PXRD) pattern shown in Fig. 2. To introduce CuO NS into GO membranes, a simple layer-by-layer (LBL) process was carried out for the membrane preparation. Filtration of CuO NS and GO solution constituted the two steps in one cycle and formed CuO NS@GO MMMs with different layers (HKUST-1@GO-*x*, where *x* indicates the number of cycles). As seen in the SEM, EDS mapping, and TEM results shown in Fig. 3, the CuO NS were evenly distributed in the MMMs. More top-view SEM images in Supplementary Figure 2 suggested the flat surface of MMMs with varied layers. For the structure information of CuO NS@MMMs, the corresponding intensity peaks for the membranes were recorded in the PXRD patterns (Fig. 3a). Beside the peaks of substrates, no obvious peaks attributable to CuO were found owing to the small amount of CuO in the

system[45]. The obtained membrane was scraped from the substrates and dispersed in ethanol for AFM characterization. As shown in Fig. 3f, the 2D morphology was maintained after mixing with GO layers, which should be a key factor for the success of ultra-thin membrane fabrication. For comparison, two more routes were applied. (1) GO, CuO NS, and BTC were dispersed in divided solution, and filtered to the nylon support alternately (HKUST-1@GO-t). However, the size of the obtained HKUST-1 crystals was too large to affect the 2D structure of the membrane. (2) As-synthesized CuO NS was mixed with exfoliated GO solution and filtered into membranes, referred to as membrane of direct mixing (HKUST-1@GO-d). Unfortunately, the mixture formed a flocculent precipitate due to the electrostatic attraction between GO and CuO NS, resulting in uneven GO and agglomeration. This phenomenon caused transformed uneven membrane, and affected the gas separation performance.

In the next step, the CuO NS embedded in MMMs were transformed to HKUST-1 via the BTC solution passing through the MMMs during the filtration process. The conversion process of powder samples can occur completely within 1 h at room temperature. For the case of CuO NS @GO membrane, the in situ reaction step induced by vacuum filtration lasted overnight due to the narrow interspacing of GO layers. The color of the membrane was changed from beige to light green after the transformation. Because of the nanodomain effect, the nanosizes were maintained during the in situ transformation process, which was proved by the SEM, EDS mapping, TEM, and AFM images in Fig. 4 and

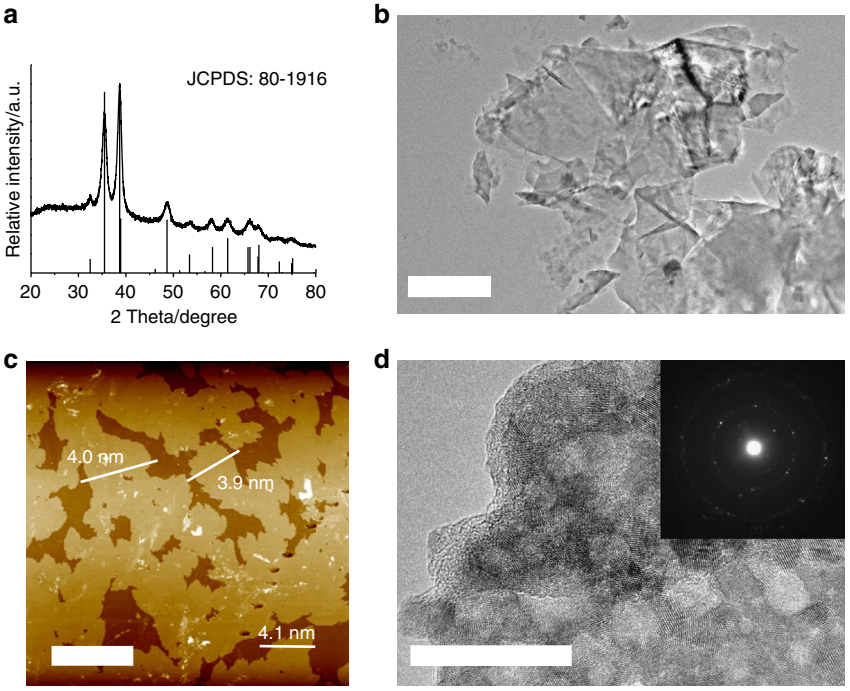

Fig. 2 Characterization of CuO NS. **a** PXRD, **b**, **d** TEM, and **c** AFM, and inside of **d** electron diffraction patterns of as-synthesized CuO NS. Scale bars, 1 μm **b**, 5 μm **c**, and 20 nm **d**

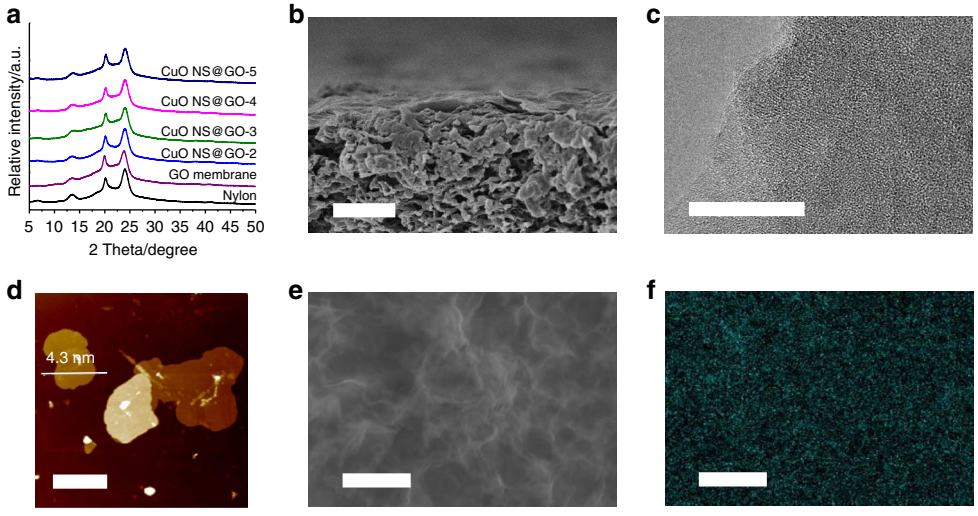

Fig. 3 Characterization of the membranes based on CuO NS and GO. **a** PXRD, **b** cross-section SEM, **c** TEM images, **d** AFM, **e** top view SEM, and **f** EDS mapping of CuO NS@GO MMMs. Scale bars, 5 μm **b**, **d**, **e**, and **f**, 20 nm **c**

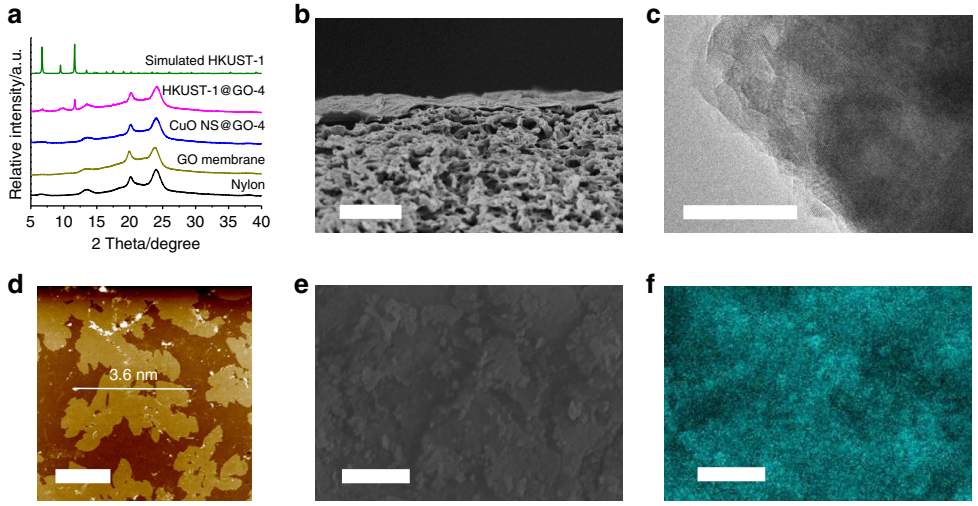

Fig. 4 Characterization of the membranes based on HKUST-1 and GO. **a** PXRD, **b** cross-section SEM, **c** TEM, **d** AFM, **e** top view SEM image, and **f** EDS mapping of HKUST-1@GO MMMs. Scale bars, 5 μm **b**, **d**, **e**, and **f**, 20 nm **c**

Supplementary Figure 3. For the HKUST-1@GO-5 MMMs, larger crystals were observed on the surface of the membrane, which may deteriorate gas separation performance of membranes. As shown in Fig. 4a and Supplementary Figure 4, peaks at 6.72°, 9.50°, and 11.44° in the PXRD patterns indicate the successful transformation to HKUST-1. The transformation was further proved by the FTIR as well (Supplementary Figure 5). Compared with the spectrum of CuO NS@GO, the peaks at 730, 1366, and 1448 cm^{-1} appear after the formation of HKUST-1, which are attributed to the symmetric stretching of the carboxylate groups in BTC (1366 and 1448 cm^{-1}) and the out-of-plane vibrations of BTC (730 cm^{-1})[46].

The cross-section SEM images are illustrated in Supplementary Figure 6 and 7; the thickness of both CuO NS@GO and HKUST-1@GO-*x* MMMs with 2–5 layers presented an ultra-thin membrane of around 100–300 nm thickness, which was lower than that of HKUST-1@GO-t and HKUST-1@GO-d membranes. There is no obvious change in the thickness of CuO NS@GO and HKUST-1@GO-*x* MMMs, which proves that the layer-by-layer combined with in situ transformation strategy was effective for the preparation of ultra-thin MOFs@GO MMMs. The EDS mapping images of cross-sections, illustrated in Supplementary Figure 8, further revealed the uniform distribution of CuO and HKUST-1 in the MMMs. X-ray photoelectron spectroscopy (XPS) tests were carried out (Supplementary Figure 9); in the spectrum of HKUST-1 powder, the Cu $2p_{3/2}$ and Cu $2p_{1/2}$ peaks are located at 935.0 and 954.9 eV, respectively[47,48]. As can be seen in the high-resolution spectrum of C 1s (Supplementary Figure 9c), the C1s peaks of HKUST-1 @GO MMMs were deconvoluted into –C–OH (286.5 eV), –COOH (288.4 eV), and –C=C–/–C–C– (284.8 eV). Compared with pristine HKUST-1 powder, the HKUST-1 @GO MMMs had one more peak: –C–OH (286.5 eV) which came from GO. This phenomenon indicates successful combination of HKUST-1 and GO. The O 1s XPS spectrum of HKUST-1 in Supplementary Figure 9d shows a major peak at a binding energy of ~532.2 eV which confirms the presence of carboxyl groups[48,49]. After HKUST-1 was integrated with GO, the binding energy of Cu $2p_{3/2}$ and Cu $2p_{1/2}$ peak in HKUST-1@GO negatively decreased by 1.8 and 1.9 eV, respectively, in comparison with those in the spectrum of pure HKUST-1 powder (Supplementary Table 1). Shifts in the C 1s, N 1s binding energies were also observed in the spectra of the HKUST-1@GO MMMs. These results provide evidence of an interaction between the HKUST-1 and GO species formed during the in situ conversion, which helped reduce the gap between two species to avoid the loss of selectivity[50]. In addition, from the Supplementary Figure 9d, the O–Cu peak (530. eV) disappeared and the –COOH peak (532.1 eV) grew up after CuO NS@GO transformed into HKUST-1 NS@GO. This phenomenon further indicates successful transformation to HKUST-1. TGA analysis was carried out on the HKUST-1@GO MMMs, and the results are shown in Supplementary Figure 10. Similar remaining weights were observed, which suggested the similar ratio of HKUST-1/GO in MMMs with different layers. The specific ratio was calculated based on TGA and precursors listed in Supplementary Table 2, and HKUST-1 ratio was obtained around 36.4 wt%. ICP tests were also performed on the HKUST-1@GO MMMs to further confirm the HKUST-1 loading amounts; the mean ratio was 39.8 wt%. The results were collected in Supplementary Table 3, which were similar to the ratios calculated from TGA results. All the characterizations above proved that HKUST-1@GO MMMs with varied thickness were successfully prepared based on the precursor of CuO NS@GO.

Gas separation properties of the HKUST-1@GO membranes. Porous environments of obtained materials were evaluated by physical gas adsorption. Brunauer–Emmett–Teller (BET) surface areas of GO, CuO NS@GO, and HKUST-1@GO MMMs were calculated on the N_2 adsorption isomers at 77 K (Fig. 5a). Compared with pristine GO, the BET surface area of HKUST-1@GO MMMs increased significantly. The enhanced free volume of membrane benefits the diffusion of gas molecules. H_2 and CO_2 adsorption curves at 273 and 298 K for GO, CuO NS@GO, and HKUST-1@GO MMMs are shown in Fig. 5b and Supplementary Figure 11. After the doping of HKUST-1, heat of adsorption for CO_2 is improved due to the affinity between the metal sites of HKUST-1 and CO_2. These properties would enhance the selectivity of MMMs as CO_2 can be attached and hindered by the involved HKUST-1.

Encouraged by the flexibility, ultra-thin membrane thickness, and gas selective adsorption, gas separation tests were applied to pure GO, CuO NS@GO, and HKUST-1@GO MMMs. Single gas permeance on GO and HKUST-1@GO MMMs was evaluated, and the results are shown in Supplementary Figure 12. Contrasting to GO membrane, the HKUST-1@GO MMMs exhibit remarkable increase in gas permeation selectivity, and hold at an acceptable H_2 permeance. The enhanced H_2/CO_2 ideal

separation factor is caused by the selective adsorption of CO_2 contributed by HKUST-1.

Furthermore, separation tests of mixture gases were carried out on the membranes using the Wicke–Kallenbach technique with an on-line gas chromatography at 25 °C (Fig. 6, Supplementary Figure 13, Supplementary Figure 14 and Supplementary Table 4). Compared with pure GO membrane and CuO NS@GO MMMs, the transformed membrane possesses significantly improved performance, which proved that the doping porous filler of HKUST-1 is beneficial for gas separation. The selectivity was enhanced by 6-fold to 73.2, while permeance achieves 5.77×10^{-7} mol m^{-2} s^{-1} Pa^{-1}. The MMMs prepared by different strategies show different gas permeation properties due to the structure and morphology (Supplementary Figure 13). Because of the uneven distribution and bulk crystals, the HKUST-1@GO MMM-t and HKUST-1@GO MMM-d, contrasted with HKUST-1@GO-4 MMMs, show larger layer gaps between GO (Supplementary Figure 7), which lead to low selectivity and higher permeance. The effect of the cycle numbers on the membrane properties was evaluated as well. The HKUST-1@GO membranes with different thickness were fabricated via varied filtration cycles, and three membranes were prepared for each thickness to take the mixed

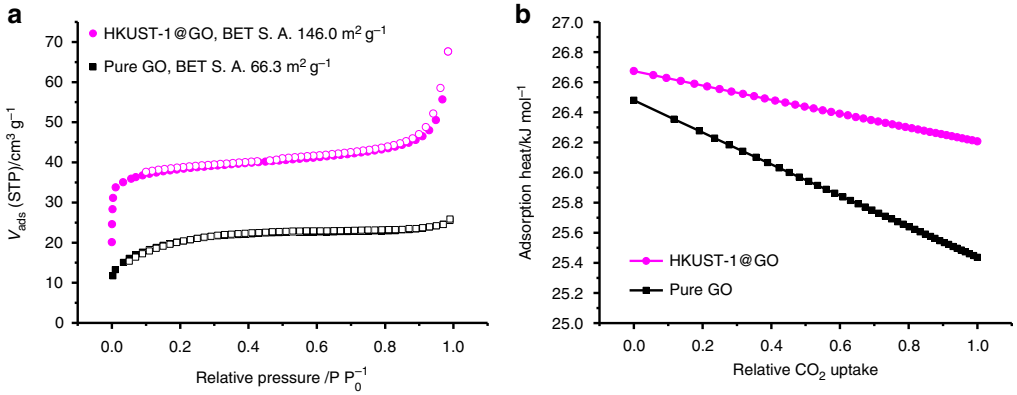

Fig. 5 Gas sorption tests of the membranes. **a** N_2 adsorption and desorption isomers for GO and HKUST-1@GO at 77 K (closed, adsorption; open, desorption); **b** adsorption heat of CO_2 for GO and HKUST-1@GO

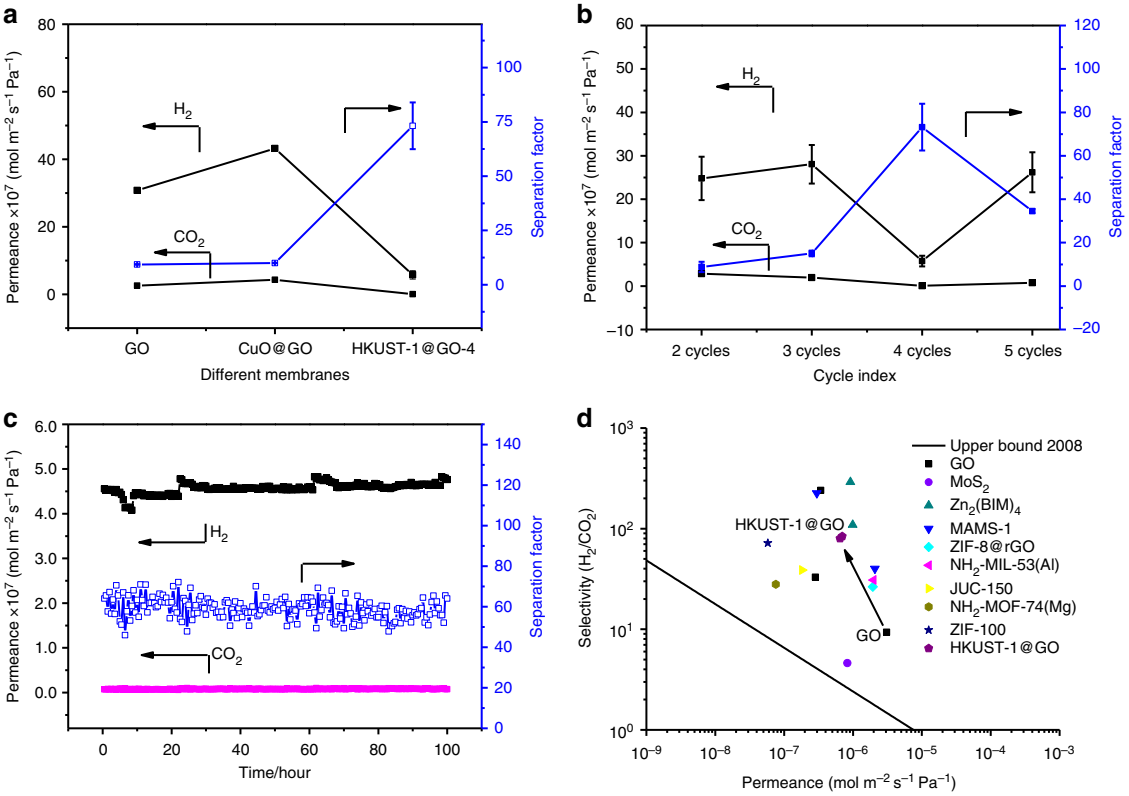

Fig. 6 Mixed gas separation performance of the membranes. **a** H_2/CO_2 mixed gases separation performances on GO membrane, CuO NS@GO-4 MMMs and HKUST-1@GO-4 MMMs. **b** H_2/CO_2 mixed gases separation performances on the HKUST-1@GO MMMs with different layers at 25 °C. Error bars denote standard deviation. **c** plot of H_2/CO_2 permeance and separation factors for the HKUST-1@GO MMMs with 4 layers versus test time. **d** H_2/CO_2 selectivity as a function of H_2 permeability for HKUST-1@GO-4 MMMs compared with other MOF and 2D membranes reported in the literature[21, 24, 27, 51–57]. The upper bound lines for polymer membranes for H_2/CO_2 are plotted according to reference[5], assuming a membrane thickness of 200 nm. Refer to Supplementary Table 5 for detailed values of the presented data points

gases separation tests. As shown in Fig. 6b, the membrane with more layers exhibits higher selectivity due to fewer defects in the thicker membranes, while the thicker membranes result in lower permeance. The HKUST-1@GO MMM-4 MMMs have both high permeance (5.77×10^{-7} mol m^{-2} s^{-1} Pa^{-1}) and selectivity ($H_2/CO_2 = 73.2$). A downgraded separation performance was detected for the HKUST-1@GO-5, which may be caused by the larger crystals grown in the MMMs (Fig. 4a and Supplementary Figure 3). To examine the stability of separation performance, the HKUST-1@GO-4 MMMs were continuously evaluated for the separation of equimolar H_2/CO_2 mixture up to 120 h without noticeable performance loss (Fig. 6c), indicating its excellent stability for long-term continuous operations. Mixture gases separation tests were also carried out on the MMMs at higher temperature of 100 °C (Supplementary Figure 14). Increased permeance and slightly decreased selectivity are obtained due to the enhanced molecular motility, proving the thermal stability of membranes. We have evaluated the gas separation performance of the HKUST-1@GO-4 membrane after bending and recovery as well, the permeance and selectivity are 6.19×10^{-7} mol m^{-2} s^{-1} Pa^{-1} and 53.5, respectively. The membrane after bending and recovery possesses a similar permeance and only a slight decline in selectivity is noted compared with the original membrane, which proves the flexibility of the composite membrane.

Due to the higher critical temperature and larger dynamic diameter of CO_2 compared with H_2, the H_2/CO_2 mixtures are a challenge to separation on polymer membrane as described in the revised Robeson upper bound relationship. As shown in the Fig. 6d, the performance of GO-based membranes in this work has surpassed the trade-off line of polymeric membranes. Compared with high-quality polycrystalline and other 2D membranes in the reference, the intercalated membrane shows both desired permeance and selectivity. A significant improvement in selectivity is achieved for HKUST-1@GO membrane by involving the microporous MOF fillers.

Discussion

Flexible CuO NS@GO MMMs were prepared by a layer-by-layer method, and transformed to HKUST-1@GO MMMs by reacting with BTC linker in situ. This strategy helps to uniformly disperse MOF in the GO matrix to maintain 2D morphology. The membrane shows significantly enhanced performance for gas separation of H_2/CO_2 mixtures. In addition, the layer cycles on the HKUST-1@GO-4 MMMs were optimized to obtain both high permeance (5.77×10^{-7} mol m^{-2} s^{-1} Pa^{-1}) and selectivity ($H_2/CO_2 = 73.2$) on HKUST-1@GO-4 MMMs. The flexibility and easy fabrication process help these membranes overcome the interfacial defects common in polycrystalline membranes. This approach can prepare larger-scale membranes with greater ease than traditional hydrothermal/solvothermal methods. Our membrane at present is more effective for a relatively small-scale dry 50:50 H_2:CO_2 feed at low pressures near atmospheric pressure. It is still challenging to prepare stable and easy processing membranes with high performance for high pressure and elevated temperature application. Thanks to the various metal centers in the MOF materials, this facile approach may be widely extended to introduce other MOFs with tailored structures into this novel type of flexible membrane for enhanced gas separation.

Methods

Materials. All the chemicals were used as received. GO powder was purchased from XF NANO, China.

Preparation of CuO NS@GO MMMs via LBL process. In a typical process, a certain volume of 2.0 mmol L^{-1} $Cu(NO_3)_2$ aqueous solution was mixed with an equal volume of 1.6 mmol L^{-1} 2-aminoethanol aqueous solution with stirring for 1 min. Then the mixed solution was aged for 24 h at a constant temperature of 25 °C. As a result, CuO NS dispersion solution was obtained, which was diluted to 1/3 concentration with DI water, giving solution A. The GO solution with the concentration of 2 mg L^{-1} was used as solution B. CuO NS@GO MMMs were prepared via a layer-by-layer filtration process on the support of nylon filter with 5.0 mL solution A/B alternately. The thickness of MMMs was controlled through varying filtration cycles, giving CuO NS@GO-x (x is the number of cycles); 25.0 mL solution B was filtered to give pure GO membrane as a comparison.

Preparation of HKUST-1@GO MMMs. HKUST-1@GO MMMs were achieved by in situ conversion in the filtration process of 25.0 mL BTC solution (solution C 1.0 mmol L^{-1} in H_2O/ethanol solution) using CuO NS@GO MMMs. The color of the membrane switched from brown to green in the filtration process, giving the HKUST-1@GO-x MMMs.

Preparation of HKUST-1@GO-t MMMs. Three-step layer-by-layer process was carried out by filtration of 5.0 mL solutions A/B/C sequentially in each cycle. And the juxtaposed membrane was obtained after four filtration cycles.

Preparation of HKUST-1@GO-d MMMs. MMMs were prepared by filtration of the mixture of solution A and B on the nylon supports, and then reacting with solution C to obtain HKUST-1@GO-d MMMs.

Characterization. The crystalline structure information of the CuO NS@GO and HKUST-1@GO membranes was collected on Dmax-rA PXRD. The microscopic features of these materials were characterized by a SEM (HITACHI S4800) and TEM (JEM-2100). The optical photos of the as-prepared membranes were taken by an iPhone 6 at normal camera mode. In order to obtain AFM images, samples were dripped and dried on the Si wafer and imaged on a commercial Multi Mode Scanning Probe Microscope with a NanoScope IVa controller (Digital Instruments, Santa Barbara, CA) in contact mode. After second-order flattening, all height images were directly analyzed using NanoScope Analysis software (version 1.40, Bruker) to obtain section profiles along the fibril axis. FTIR spectrums of membranes were collected by a Version-B Fourier transform spectrometer, PE. XPS experiments were performed with a Kratos AXIS Ultra DLD surface analysis instrument using a monochromatic Al Kαradiation (1486.71 eV) at 15 kV as the excitation source. BET surface area of the samples was calculated from the N_2 adsorption–desorption isothermal curve at 77 K, which was collected on Micro ASAP2020. Gas adsorption–desorption measurements of H_2 (99.995%), CO_2 (99.995%), CH_4 (99.95%), and N_2 (99.995%) on powder samples were carried out on Micro ASAP2020 at 273 and 298 K, after the samples were degassed at 423 K under vacuum overnight. For the experimental setup of gas-separation measurement, the membrane was set in a stainless steel cell at different temperatures and standard atmospheric pressure. One side of the membrane was swept by argon while the other side was exposed to single gases or gas mixtures (Supplementary Figure 15). A soap-film flow meter was used to confirm the rate of argon and feed gases before test. The membrane would be fixed by two O-rings in the cell. To prevent damage to the membrane surface caused by the contact of O-rings, the edge of the membrane was covered by foil-tape, leaving a 10-mm-diameter circular membrane surface. The mixed feed flow rates were constant with a total volumetric flow rate of 100 mL min^{-1} (with 50 mL min^{-1} of each gas, 1:1 mixture), regulated by mass flow controllers (MFCs). Argon was used as a sweep gas to minimize the influence of back diffusion of the sweeping gas to the feed side. The sweep gas flow rate was 80 mL min^{-1} to eliminate concentration polarization in the permeate side. The calibration curves were made by fitting of more than eight points each. The value of each point was based on more than 20 GC (SHIMADZU GC-2014C) parallel tests. The permeate flow rates of test gases were calculated from the corresponding GC results and calibration curves. The permeability that is termed the permeance (P_i (mol m^{-2} s^{-1} Pa^{-1})) of MOFs membrane was calculated with the following Eq. 1:

$$P_i = \frac{N_i}{\Delta p_i \times A}, \quad (1)$$

where N_i (mol s^{-1}) is the permeate flow rate of component i, Δp_i (Pa) is the trans-membrane pressure drop of i, and A (m^2) is the membrane area.

The membrane permselectivity was evaluated by separation factor ($\alpha_{i/j}$), which was obtained according to Eq. 2:

$$\alpha_{i/j} = \frac{X_i/X_j}{Y_i/Y_j}, \quad (2)$$

where i, j represent the two components in the mixture and X, Y are the mole fractions in the permeate and feed solution, respectively.

Data availability. The data that support the findings of this study are available from the corresponding author upon reasonable request.

Received: 11 September 2017 Accepted: 27 November 2017
Published online: 08 March 2018

References

1. Lin, J. Y. S. Molecular sieves for gas separation. *Science* **353**, 121–122 (2016).
2. Sholl, D. S. & Lively, R. P. Seven chemical separations to change the world. *Nature* **532**, 435–437 (2016).
3. Baker, R. W. Future directions of membrane gas separation technology. *Ind. Eng. Chem. Res.* **41**, 1393–1411 (2002).
4. Koros, W. J. & Zhang, C. Materials for next-generation molecularly selective synthetic membranes. *Nat. Mater.* **16**, 289–297 (2017).
5. Robeson, L. M. The upper bound revisited. *J. Membr. Sci.* **320**, 390–400 (2008).
6. Freeman, B. D. Basis of permeability/selectivity tradeoff relations in polymeric gas separation membranes. *Macromolecules* **32**, 375–380 (1999).
7. Sanders, D. E. et al. Energy-efficient polymeric gas separation membranes for a sustainable future: a review. *Polymer (Guildf)* **54**, 4729–4761 (2013).
8. Coronas, J. & Santamaría, J. Separations using zeolite membranes. *Sep. Purif. Rev.* **28**, 127–177 (1999).
9. Li, J. R., Kuppler, R. J. & Zhou, H. C. Selective gas adsorption and separation in metal–organic frameworks. *Chem. Soc. Rev.* **38**, 1477–1504 (2009).
10. Rangnekar, N., Mittal, N., Elyassi, B., Caro, J. & Tsapatsis, M. Zeolite membranes - a review and comparison with MOFs. *Chem. Soc. Rev.* **44**, 7128–7154 (2015).
11. Qiu, S., Xue, M. & Zhu, G. Metal–organic framework membranes: from synthesis to separation application. *Chem. Soc. Rev.* **43**, 6116–6140 (2014).
12. Kosinov, N., Gascon, J., Kapteijn, F. & Hensen, E. J. M. Recent developments in zeolite membranes for gas separation. *J. Membr. Sci.* **499**, 65–79 (2016).
13. Kang, Z., Fan, L. & Sun, D. Recent advances and challenges of metal–organic framework membranes for gas separation. *J. Mater. Chem. A* **5**, 10073–10091 (2017).
14. Askari, M. & Chung, T.-S. Natural gas purification and olefin/paraffin separation using thermal cross-linkable co-polyimide/ZIF-8 mixed matrix membranes. *J. Membr. Sci.* **444**, 173–183 (2013).
15. Zhang, C., Dai, Y., Johnson, J. R., Karvan, O. & Koros, W. J. High performance ZIF-8/6FDA-DAM mixed matrix membrane for propylene/propane separations. *J. Membr. Sci.* **389**, 34–42 (2012).
16. Zhang, C. et al. Highly scalable ZIF-based mixed-matrix hollow fiber membranes for advanced hydrocarbon separations. *AlChE J.* **60**, 2625–2635 (2014).
17. Wang, Z., Wang, D., Zhang, S., Hu, L. & Jin, J. Interfacial design of mixed matrix membranes for improved gas separation performance. *Adv. Mater.* **28**, 3399–3405 (2016).
18. Kim, W.-g. & Nair, S. Membranes from nanoporous 1D and 2D materials: a review of opportunities, developments, and challenges. *Chem. Eng. Sci.* **104**, 908–924 (2013).
19. Eng-Poh, N., Chateigner, D., Bein, T., Valtchev, V. & Mintova, S. Capturing ultrasmall EMT zeolite from template-free systems. *Science* **335**, 70–73 (2012).
20. Varoon, K. et al. Dispersible exfoliated zeolite nanosheets and their application as a selective membrane. *Science* **334**, 72–75 (2011).
21. Yuan Peng, Y. L. et al. Metal–organic framework nanosheets as building blocks for molecular sieving membranes. *Science* **346**, 1356–1359 (2014).
22. Li, H. et al. Ultrathin, molecular-sieving graphene oxide membranes for selective hydrogen separation. *Science* **342**, 95–98 (2013).
23. Jeon, M. Y. et al. Ultra-selective high-flux membranes from directly synthesized zeolite nanosheets. *Nature* **543**, 690–694 (2017).
24. Wang, X. et al. Reversed thermo-switchable molecular sieving membranes composed of two-dimensional metal–organic nanosheets for gas separation. *Nat. Commun.* **8**, 14460 (2017).
25. Joshi, R. K. et al. Precise and ultrafast molecular sieving through graphene oxide membranes. *Science* **343**, 752–754 (2014).
26. Liu, G., Jin, W. & Xu, N. Two-dimensional-material membranes: a new family of high-performance separation membranes. *Angew. Chem. Int. Ed.* **55**, 13384–13397 (2016).
27. Shen, J. et al. Subnanometer two-dimensional graphene oxide channels for ultrafast gas sieving. *ACS Nano* **10**, 3398–3409 (2016).
28. Hu, M. & Mi, B. Enabling graphene oxide nanosheets as water separation membranes. *Environ. Sci. Technol.* **47**, 3715–3723 (2013).
29. Yang, T., Lin, H., Zheng, X., Loh, K. P. & Jia, B. Tailoring pores in graphene-based materials: from generation to applications. *J. Mater. Chem. A* **5**, 16537–16558 (2017).
30. Hu, Z. et al. Kinetically controlled synthesis of two-dimensional Zr/Hf metal–organic framework nanosheets via a modulated hydrothermal approach. *J. Mater. Chem. A* **5**, 8954–8963 (2017).
31. Xu, M. et al. Two-dimensional metal–organic framework nanosheets as an enzyme inhibitor: modulation of the alpha-chymotrypsin activity. *J. Am. Chem. Soc.* **139**, 8312–8319 (2017).
32. Huang, L. et al. In situ synthesis of ultrathin metal–organic framework nanosheets: a new method for 2D metal-based nanoporous carbon electrocatalysts. *J. Mater. Chem. A* **5**, 18610–18617 (2017).
33. Guo, H., Zhu, G., Hewitt, I. J. & Qiu, S. "Twin copper source" growth of metal–organic framework membrane: Cu3(BTC)2 with high permeability and selectivity for recycling H2. *J. Am. Chem. Soc.* **131**, 1646–1647 (2009).
34. Kang, Z. et al. "Single nickel source" in situ fabrication of a stable homochiral MOF membrane with chiral resolution properties. *Chem. Commun.* **49**, 10569–10571 (2013).
35. Mao, Y. et al. Room temperature synthesis of free-standing HKUST-1 membranes from copper hydroxide nanostrands for gas separation. *Chem. Commun.* **49**, 5666–5668 (2013).
36. Guo, Y., Mao, Y., Hu, P., Ying, Y. & Peng, X. Self-confined synthesis of HKUST-1 membranes from CuO nanosheets at room temperature. *ChemistrySelect* **1**, 108–113 (2016).
37. Zhan, G. & Zeng, H. C. Synthesis and functionalization of oriented metal-organic-framework nanosheets: toward a series of 2D catalysts. *Adv. Funct. Mater.* **26**, 3268–3281 (2016).
38. Zhan, G. & Zeng, H. C. Alternative synthetic approaches for metal–organic frameworks: transformation from solid matters. *Chem. Commun.* **53**, 72–81 (2016).
39. Liu, Y. et al. Flexible CuO nanosheets/reduced-graphene oxide composite paper: binder-free anode for high-performance lithium-ion batteries. *ACS Appl. Mater. Interfaces* **5**, 9850–9855 (2013).
40. Ghosh, D., Giri, S. & Das, C. K. Preparation of CTAB-assisted hexagonal platelet Co(OH)2/graphene hybrid composite as efficient supercapacitor electrode material. *ACS Sustain. Chem. Eng.* **1**, 1135–1142 (2013).
41. Jeong, G. H., Baek, S., Lee, S. & Kim, S. W. Metal oxide/graphene composites for supercapacitive electrode materials. *Chem. Asian J.* **11**, 949–964 (2016).
42. Hsu, Y.-W. et al. Synthesis of CuO/graphene nanocomposites for nonenzymatic electrochemical glucose biosensor applications. *Electrochim. Acta* **82**, 152–157 (2012).
43. Gao, Z. et al. Synthesis and exfoliation of layered α-Co(OH)2Nanosheets and their electrochemical performance for supercapacitors. *Eur. J. Inorg. Chem.* **2013**, 4832–4838 (2013).
44. Li, Z. et al. Rapid synthesis of graphene/cobalt hydroxide composite with enhanced electrochemical performance for supercapacitors. *J. Power Sources* **245**, 224–231 (2014).
45. Zhu, J. et al. Decorating graphene oxide with CuO nanoparticles in a water-isopropanol system. *Nanoscale* **2**, 988–994 (2010).
46. Li, L. et al. A MOF/graphite oxide hybrid (MOF: HKUST-1) material for the adsorption of methylene blue from aqueous solution. *J. Mater. Chem. A* **1**, 10292–10299 (2013).
47. Jolley, J. G., Geesey, G. G., Hankins, M. R., Wright, R. B. & Wichlacz, P. L. Auger electron and x-ray photoelectron spectroscopic study of the biocorrosion of copper by alginic acid polysaccharide. *Appl. Surf. Sci.* **37**, 469–480 (1989).
48. Hall, A. S., Kondo, A., Maeda, K. & Mallouk, T. E. Microporous brookite-phase titania made by replication of a metal–organic framework. *J. Am. Chem. Soc.* **135**, 16276–16279 (2013).
49. Lopez, G. P., Castner, D. G. & Ratner, B. D. XPS 0 1s binding energies for polymers containing hydroxyl, ether, ketone and ester groups. *Surf. Interface Anal.* **17**, 267–272 (1991).
50. Dechnik, J., Gascon, J., Doonan, C. J., Janiak, C. & Sumby, C. J. Mixed-matrix membranes. *Angew. Chem. Int. Ed.* **56**, 2–21 (2017).
51. Li, W. et al. Metal–organic framework channelled graphene composite membranes for H2/CO2 separation. *J. Mater. Chem. A* **4**, 18747–18752 (2016).
52. Chi, C. et al. Facile preparation of graphene oxide membranes for gas separation. *Chem. Mater.* **28**, 2921–2927 (2016).
53. Wang, D., Wang, Z., Wang, L., Hu, L. & Jin, J. Ultrathin membranes of single-layered MoS(2) nanosheets for high-permeance hydrogen separation. *Nanoscale* **7**, 17649–17652 (2015).
54. Zhang, F. et al. Hydrogen selective NH2 -MIL-53(Al) MOF membranes with high permeability. *Adv. Funct. Mater.* **22**, 3583–3590 (2012).
55. Kang, Z. et al. Highly selective sieving of small gas molecules by using an ultra-microporous metal–organic framework membrane. *Energy Environ. Sci.* **7**, 4053–4060 (2014).
56. Wang, N., Mundstock, A., Liu, Y., Huang, A. & Caro, J. Amine-modified Mg-MOF-74/CPO-27-Mg membrane with enhanced H2/CO2 separation. *Chem. Eng. Sci.* **124**, 27–36 (2015).
57. Wang, N. et al. Polydopamine-based synthesis of a zeolite imidazolate framework ZIF-100 membrane with high H2/CO2 selectivity. *J. Mater. Chem. A* **3**, 4722–4728 (2015).

Acknowledgements

This work was supported by National Natural Science Foundation of China (21501198, 21601205, 21371179, 21571187) and Taishan Scholar Foundation (ts201511019).

Author contributions

All authors contributed extensively to the work presented in this manuscript. D.S. and Z.K. formulated and supervised the project. Z.K. prepared HKUST-1@GO membranes and performed PXRD and gas permeation tests. Z.K. and H.G. performed SEM and TEM tests. M.Z. and R.W. collected the gas sorption results of membranes. L.F., J.P. and X.D. performed AFM. S.W. carried out the FTIR and TGA tests. S.W. and W.K. performed the XPS study. S.W. and Z.K. collected the gas separation results of membranes. Z.K. and D.S. wrote the paper, and L.F. contributed to revising the paper. D.S., R.W., Z.K. and L.F. financed the project.

Additional information

Supplementary information is available for this paper at https://doi.org/10.1038/s42004-017-0002-y.

Competing interests: The authors declare no competing financial interests.

Reprints and permission information is available online at http://npg.nature.com/reprintsandpermissions/

Publisher's note: Springer Nature remains neutral with regard to jurisdictional claims in published maps and institutional affiliations.